Friction-induced vibration for an aircraft brake system–Part 1: Experimental approach and stability analysis

Jean-Jacques Sinou, Olivier Dereure, Guy-Bernard Mazet, Fabrice Thouverez, Louis Jezequel

Journal home page : http://www.sciencedirect.com/science/journal/00207403

Friction-induced vibration for an aircraft brake system—Part 1: Experimental approach and stability analysis
International Journal of Mechanical Sciences, Volume 48, Issue 5, May 2006, Pages 536-554
J.-J. Sinou, O. Dereure, G.-B. Mazet, F. Thouverez and L. Jezequel

FRICTION INDUCED VIBRATION FOR AN AIRCRAFT BRAKE SYSTEM. PART 1 : EXPERIMENTAL APPROACH AND STABILITY ANALYSIS

J-J. SINOU [1*], O. DEREURE [2] , G-B. MAZET [2] , F. THOUVEREZ [1], and L. JEZEQUEL [1]

[1]Laboratoire de Tribologie et Dynamique des Systèmes UMR CNRS 5513
Ecole Centrale de Lyon,69134 Ecully, France.
[2]Messier-Bugatti, Aircraft Braking Division, Zone Aéronautique Louis Bréguet
BP 40, 78140 Vélizy-Villacoublay, France.

ABSTRACT

Friction induced vibrations are a major concern in a wide variety of mechanical systems. This is especially the case in aircraft braking systems where the problem of unstable vibrations in disk brakes has been studied by a number of researchers. Solving potential vibration problems requires experimental and theoretical approaches.
A nonlinear model for the analysis of mode aircraft brake whirl is presented and developed based on experimental observations. The non-linear contact between the rotors and the stators, and mechanisms between components of the brake system are considered.
Stability is analyzed by determining the eigenvalues of the Jacobian matrix of the linearized system at the equilibrium point. Linear stability theory is applied in order to determine the effect of system parameters on stability.

1 INTRODUCTION

An aircraft brake system is given in Figure 1. As shown, the brake is composed of a stack of rotating brake discs (rotors) which engage the wheel, and stationary brake discs (stators), which engage the torque tube. The torque tube is attached to the piston housing that links to the landing gear through a torque take-out rod. During operation, the brake is activated by the hydraulic system pressure, which compresses the heat stack: the rotors and the stators are squeezed together by hydraulic pistons and the brake produces torque by virtue of friction forces generated at the rubbing interface between the rotors and the stators. Then, vibration can be further induced by the friction characteristics of the heat sink material.
Two important specific complex nonlinear phenomena have been identified: squeal and whirl. The other major vibration modes are gear walk and chatter. *Gear walk* is defined as the cyclic fore and aft motion of the landing gear assembly. The frequency spectrum of gear walk is in the 5 – 20 Hz range. *Chatter* is defined as a torsional motion of the rotating parts of the brake-wheel-tire assembly about the axle and against the elastic restraint of the tire. The frequency spectrum of chatter is in the 50-100 Hz range. *Squeal* is defined as torsional vibrations of non-rotating brake parts around the axle. The frequency spectrum of squeal is in the 100 – 1000 Hz range. *Whirl* is defined as a motion/mode wherein the cantilevered end of the torque plaque orbits about the axle accompanied by unphased pumping of the brake pistons. Brake whirl mode within the same frequency range as brake squeal (200-300 Hz range) and can couple parametrically. Hydraulic damping provided by the piston housing fluid circuit represents a prime source of whirl damping. If the hydraulic damping provided by the piston housing fluid is insufficient, orifices may be used to increase damping to required levels.

The goal of this study is to present an analysis of the whirl vibration in aircraft brake system. A simplified aircraft braking system and parametric studies are used in order to understand the stable and unstable behavior of the aircraft brake system.
First, some basic concepts of aircraft brake systems will be introduced. Second, experimental tests and their results will be presented, in which a combination of experimental and analytical techniques are employed in order to solve potential vibration problems.
Next, a model for analyzing whirl mode vibration in aircraft braking systems will be presented. The model considers the non-linear contact between the rotors and the stators and some mechanisms between the components of the brake system. This model does not use brake negative damping and predicts that system instability can occur with a constant brake friction coefficient. Then, results from stability analyses and parametric studies using this model will be presented. System stability can be altered by changes in the brake friction coefficient, pressure, the sprag-slip mechanism, geometry and various brake design parameters. More particularly, it will be demonstrated that adding damping may change the stability of the aircraft brake system and may have disastrous effects on the stability analysis.

2 EXPERIMENTAL APPROACH

Tests of brake systems can be conducted using a roadwheel dynamometer which is a large rotating mass simulating aircraft inertia, as illustrated in Figure 2. The roadwheel dynamometer is brought up to speed. Then, the wheel and brake system are set on this roadwheel. Finally, the brakes are activated by the hydraulic system pressure, which compresses the heat stack. The roadwheel dynamometer is stopped. This test is a simulation of aircraft brake stopping.
A series of tests with a fully instrumented aircraft brake (51 accelerometers) is performed in order to analyze precisely the mechanisms of the main resonances appearing on this brake in the 0-1000 Hz frequency range. In particular, the torque tube was instrumented with accelerometers. Figure 3 shows the accelerometer locations on each instrumented part. A typical example of a torque tube signal evidencing the whirl mode is presented in Figures 4 and 5. Figures 6 and 7 illustrate the large amplitude of pressure oscillations at the piston housing due to the whirl phenomenon. Due to this instability, the amplitude oscillation of the signal increases and the whirl instability appears between 240 and 280Hz, as illustrated in Figure 5 and Figure 7. This instability may be associated with “whirl” vibrations by considering the experimental vibrations of the aircraft brake system. The typical deformation of the entire aircraft brake system due to the experimental instability is given in Figure 8. Markers from ① to ⑥ indicate the evolution of deformation of the brake system for one period. All accelerometer locations on the aircraft brake system are given again in the last image of Figure 8. An axial deflection of the axle tube and a complex rotating-bending motion of the brake may be observed (indicated by the whirling motion of the torque plate and the piston housing at the top and bottom of the aircraft brake system from marker ① to ⑥). This complex rotating-bending mode of the brake and axle around 200-300Hz due to the wobble-type plate motion of the brake friction stack coupled with the axle bending in two perpendicular planes is defined as the standard whirl mode [1-3].

3 THEORETICAL APPROACH

In this section, an analytical model will be developed based on the previous experimental observations in order to reproduce the whirl instability. First, the whirl description and modeling will be presented based on the previous experimental approaches. Second, the mechanism of friction-induced vibration will be introduced in order to model the contact at the interface between rotors and stators of the aircraft brake system. Then, the non-linear behavior of the rotor/stator stack will be investigated and the complete whirl modeling will be established.

3.1 Whirl modeling

Friction-induced vibration has been described and analyzed in a number of published studies of varying complexity. In a previous work, Ozbek et al.[1-2] and Gordon [3] present whirl vibration as a wobbling motion between the brake’s rotating and stationary parts. Whirl can be detected by piston pressure oscillations. Feld and Fehr [4] explain whirl vibration: the disks in the brake stack are compressed by the hydraulic pressure applied to

the brake, as illustrated in Figure 9. Without vibration, the normal pressure is distributed uniformly over the rubbed surface between rotating and stationary disks. When vibration is present, disks in the brake stack are subjected to out-of-plane rotation called accordion motion. The uniform normal pressure over the disk interface is then altered by this accordion motion: the normal pressure increases over half of the interface and relaxes over the other half. Moreover, the friction force varies proportionally to this normal pressure and produces the whirl motion [5].

Considering the previous experimental results (illustrated in Figure 8), it has been observed that lateral displacement and rotations in two perpendicular planes of the rotor and stator appear. Figure 4 and 5 indicate rotation of the piston housing. Figure 8 shows that the axle bending and rotation of the stator's and rotor's shaft are important. So, the retained degree of freedom for the modeling of the whirl instability are

- the rigid body lateral displacement of the rotor and stator: x_s and x_r,
- the stator rigid body yaw rotation in the two perpendicular planes: θ_s and ψ_s,
- the rotor rigid body yaw rotation in the two perpendicular planes: θ_r and ψ_r,
- the piston housing rigid torsional rotation φ_s,
- the axle deflection and axle bending rotation of the axle stator's shaft in the two perpendicular planes: y_a, z_a, θ_a and ψ_a,
- the axle deflection and axle bending rotation of the axle rotor's shaft in the two perpendicular planes: y_b, z_b, θ_b and ψ_b

Finally, the vector of degree of freedom for the aircraft brake system is defined by

$$\mathbf{x} = \left\{ x_s \quad \theta_s \quad \psi_s \quad \varphi_s \quad x_r \quad \theta_r \quad \psi_r \quad y_b \quad \theta_b \quad z_b \quad \psi_b \quad y_a \quad \theta_a \quad z_a \quad \psi_a \right\}^T \qquad (1)$$

Before writing the global equation of motion of the aircraft brake system, the mechanism of friction and the contact at the rotor/stator interface will be investigated.

3.2 Mechanism of friction-induced vibration for an aircraft brake system

In this section, the general mechanisms of friction-induced vibration are developed and more particularly the sprag-slip phenomenon and the associated geometric coupling are evaluated. Friction-induced vibration occurs in many industrial applications with rotating and sliding parts and is undesirable due to its detrimental effects on the performance of mechanical systems and its role on the accelerated wear of components, damage and noise. Different types of vibrations induced by friction have been studied in the past by several researchers: Ibrahim [6-7], Crolla and Lang [8], and Kinkaid et al. [9] provide an extensive study of many aspects of friction-induced vibration. Moreover, the contact forces between two surfaces play an important role in self-excited vibrations: cf. Oden and Martins [10] proposed review of frictional contact of metallic surfaces. The different mechanisms of friction-induced vibration fall into four classes: stick-slip, variable dynamic friction coefficient, sprag-slip and geometric coupling of degrees of freedom. In this study, we will consider the latter two approaches that use modal coupling to develop instability when the friction coefficient is constant.

The first two approaches rely on using the changes in the friction coefficient: the stick-slip is a low sliding speed phenomenon caused by the static friction coefficient being higher than the dynamic friction coefficient. The simple system which has been used to examine the stick-slip phenomenon, is that of a mass sliding on a moving belt. Stick-slip motion is seen to depend on the speed of kinematic friction and produce self-excited vibration.

The 1960s saw new developments of mechanisms for friction-induced vibration and the introduction of sprag-slip motions and geometric coupling. In 1961, Spurr [11] proposed a mechanism for friction-induced vibrations which is known as sprag-slip. Consider a strut inclined at an angle θ to a sliding surface, as illustrated in Figure 10(a). The magnitude friction force is given by

$$F = \frac{\mu L}{1 - \mu \tan\theta} \qquad (2)$$

where μ defines the coefficient of friction and L the load. It is seen that when μ approaches $\cot\theta$, the friction force F approaches infinity. When $\mu = \cot\theta$, the strut sprags or locks and motion becomes impossible. However, by introducing the second section $O'O"$, as shown in Figure 10(b), Spurr releases the sprag through the new equivalent angle θ'. The arm rotates about the elastic pivot O'. If the moment opposing the rotation about O' becomes so large that $PO'O"$ becomes equivalent to a rigid strut $PO"$. In this case, $O"$ becomes the primary pivot point and the incline angle θ' is reduced to $\theta"$. The elastic energy stored in O' can now be released: $O'P$ swings off the surface; this produces slip and the cycle then repeats itself .

The last mechanism involves the coupling of the different degrees of freedom. It is an extension of the sprag-slip model and requires at least two degrees of freedom. This phenomenon was first demonstrated by Jarvis and Mills [12] in a pioneering study of a cantilever-disk system. It was the first approach attempting to mathematically simulate an experimental system. Following this work, several authors have made contributions to support this theory of geometric coupling. Earles and Soar [13] conducted extensive studies on squealing pin-disk systems; Millner [14] and North [15] theoretically demonstrated that geometric coupling could cause brake squeal. D'Souza and Dweib [16] attributed friction vibration of their pin-disk system to the coupling of vibrations. These studies have illustrated that frictional instability can be caused by geometrically induced instabilities that do not require variations in the coefficient of friction.

For an aircraft brake system, component clearances within the brake can affect dynamic system stability. This is why understanding this mechanism is an important element of the analytical model [6-16]. On some gear systems, the brake rod attaches to the brake housing in an offset, cantilevered fashion such that the rod operates out-of-plane with the hydraulic system. Due to this offset, an angle β may appear between the brake rod and the housing, as shown in Figure 11. This offset angle β couples the normal and tangential contact force and introduces kinematic constraints and modal coupling to develop the instability [7-9]. This coupling is one of the primary causes of instability for whirl vibration. In this case, instability can occur with a constant brake friction coefficient.

3.3 Nonlinear contact stress

Experimental results (static tests, as illustrated in Figure 12) have shown that the load-deflection relationship is highly non-linear. One assumes that the non-linear normal stress F acting at the interface surface between the stator and rotor can be expressed as a cubic polynomial in the relative displacement between the rotor and stator in compression

$$F = \sum_{i=1}^{3} K_i \delta x^i \tag{3}$$

where δx is the relative displacement between the rotor and stator. This assumption is verified by static tests, as illustrated in Figure 12: the non-linear relationship between load and deflection is used to determine the non-linear coefficients K_i $(i = 1, 2 \text{ and } 3)$. As shown in Figure 13, there is good agreement with the experimental non-linear contact stress and the cubic polynomial solution.

3.4 Friction interface

Assuming that the tangential stress T is generated by the brake friction coefficient μ, we now take into account the Coulomb friction. The multi-stage brake is represented by a single rotor, as illustrated in Figure 14, and stator with the effective brake friction coefficient $\mu_{total} = 2N\mu$ where N is the number of interfaces between stators and rotors. It is assumed that the rotor and stator friction surfaces are always in contact. In this whirl system, we take into account the rigid body lateral displacement and the two yaws of the stator and rotor. For any point $M(r,\theta)$ on the rotor and stator, and taking into account small displacements, the normal displacement of the rotor and the stator are

$$\begin{cases} x_{rotor}(r,\theta) = x_r - r\sin\theta\sin\theta_r - r\cos\theta\sin\psi_r \approx x_r - r\theta_r\sin\theta - r\psi_r\cos\theta \\ x_{stator}(r,\theta) = x_s - r\sin\theta\sin\theta_s - r\cos\theta\sin\psi_s \approx x_s - r\theta_s\sin\theta - r\psi_s\cos\theta \end{cases} \quad (4)$$

where x_s, x_r, θ_s, θ_r, ψ_s and ψ_r are the stator and the rotor lateral displacement, and the stator and rotor rotations, as illustrated in Figure 14. Then, for any point $M(r,\theta)$ on the disk surface, the normal displacement is

$$x(r,\theta) = x_{stator}(r,\theta) - x_{rotor}(r,\theta) = (x_s - x_r) - r\sin\theta(\theta_s - \theta_r) - r\cos\theta(\psi_s - \psi_r) \quad (5)$$

The normal force F_X due to the normal contact between the rotor and the stator friction surface, and the moments M_X, M_Y and M_Z are given by

$$F_X = \int_0^{2\pi}\int_{Ri}^{R0} N(r,\theta)\,r\,dr\,d\theta \quad (6)$$

$$M_X = \int_0^{2\pi}\int_{Ri}^{R0} T(r,\theta)\,r^2\,dr\,d\theta = \int_0^{2\pi}\int_{Ri}^{R0} \mu N(r,\theta)\,r^2\,dr\,d\theta \quad (7)$$

$$M_Y = -\int_0^{2\pi}\int_{Ri}^{R0} N(r,\theta)r^2\sin\theta\,dr\,d\theta \quad (8)$$

$$M_Z = -\int_0^{2\pi}\int_{Ri}^{R0} N(r,\theta)r^2\cos\theta\,dr\,d\theta \quad (9)$$

The force and moments due to the friction at the rotor/stator interface are indicated in Figure 14.

3.5 Equations of motion

In this section, the global equation of motion for the whirl will be established. As explained previously, the vector of the degree-of-freedom is given by

$$\mathbf{x} = \{x_s \quad \theta_s \quad \psi_s \quad \varphi_s \quad x_r \quad \theta_r \quad \psi_r \quad y_b \quad \theta_b \quad z_b \quad \psi_b \quad y_a \quad \theta_a \quad z_a \quad \psi_a\}^T \quad (10)$$

where x_s, x_r, θ_s, θ_r, ψ_s, ψ_r, φ_s, y_a, z_a, θ_a, ψ_a, y_b, z_b, θ_b and ψ_b are the stator and the rotor lateral displacement, the stator and rotor rotations, the piston torsional rotation and the axle deflections and rotations of the stator and rotor shaft, respectively.

First, normal hydraulic pressure is applied at the left side of the stator rigid body in the X-direction as illustrated in Figure 14. The vector associated with the hydraulic pressure is given by

$$\mathbf{F}_{\mathbf{pressure}} = \{F_{hyd/X} \quad 0 \quad 0 \quad 0 \quad 0 \quad 0 \quad 0 \quad 0 \quad 0 \quad 0 \quad 0 \quad 0 \quad 0 \quad 0 \quad 0\}^T \quad (11)$$

where $F_{hyd/X}$ is the brake force due to the hydraulic pressure, as indicated in Figure 15. It is given by

$$F_{hyd/X} = P_{hydraulic} n_{piston} \frac{\left(R^2_{piston/outer} - R^2_{piston/inner}\right)}{\left(R_0^2 - R_i^2\right)} \quad (12)$$

where n_{piston}, $R_{piston/outer}$, $R_{piston/inner}$ are the number of pistons, the outer and inner radius of the piston surface in contact with the stator, respectively. R_0 and R_i define the outer and inner radius of the rotor/stator interface, respectively.

Then, considering the previous expressions (6-9) of the normal friction force and friction moment due to the contact at the rotor/stator interface, the vector associated with the contact friction expressions is given by

$$\mathbf{F}_{\mathbf{contact}} = \{-F_X \quad M_Y \quad M_Z \quad M_X \quad F_X \quad -M_Y \quad -M_Z \quad 0 \quad 0 \quad 0 \quad 0 \quad 0 \quad 0 \quad 0 \quad 0\}^T \quad (13)$$

The normal force and moments are completely defined in Figures 14 and 15. The complete expressions are given in equations (6-9)

Then, the load due to the brake rod (indicated in Figure 15) is given by

$$\mathbf{F}_{\mathbf{couple}} = \{0 \quad F_{couple/Z}d_e + F_{couple/X}R_e \quad F_{couple/Y}d_e \quad -F_{couple/Y}R_e \quad 0 \quad 0 \quad 0 \quad 0 \quad 0 \quad 0 \quad 0 \quad 0 \quad 0 \quad 0 \quad 0\}^T \quad (14)$$

where $F_{couple/X}$, $F_{couple/Y}$ and $F_{couple/Z}$ represent the load due to the brake rod, as indicated in Figures 14 and 15. d_e and R_e represent the brake rod lateral offset and the axle to brake rod axis distance, as indicated in Figures 14 and 15.

Considering the offset angle (Figure 11), the complete expressions due to the brake rod are

$$\begin{cases} F_{couple/X} = K_{rod} R_e \phi_s \sin\alpha + K_{rod} x_s \sin\alpha + K_{rod} R_e \theta_s \sin\alpha \\ F_{couple/Y} = K_{rod} R_e \phi_s \cos\alpha - K_{rod} d_e \theta_s \cos\alpha \\ F_{couple/Z} = K_{rod} R_e \phi_s \cos\alpha - K_{rod} d_e \psi_s \cos\alpha \end{cases} \tag{15}$$

where K_{rod} defines the axial stiffness of the brake rod and α is the offset angle due to the brake rod angle with the rotor/stator interface.

Finally, interconnections between each element of the aircraft brake system need to be taken into account in order to established the complete equations of motion. First, the stator and the shaft of the stator interact via notches on the inner perimeter of the disk, and the rotor and the shaft of the rotor interact via drive keys on the outside of the disk as illustrated in Figure 15. Moreover, the right side of the rotor is retained by the backplate of the brake and torque plate (with the associated stiffness K_{rr}), as indicated in Figure 15. The left side of the stator is retained by the hydraulic element (with the associated stiffness K_{hyd}), as illustrated in Figure 15.

Finally, by considering these interconnections between each element and the classical structural mass, damping and stiffness matrices of the aircraft brake system, the global non-linear expression is given as

$$\mathbf{M}\ddot{\mathbf{x}} + \mathbf{C}\dot{\mathbf{x}} + \mathbf{K}\mathbf{x} = \mathbf{F}_{\mathbf{pressure}} + \mathbf{F}_{\mathbf{couple}}(\mathbf{x}) + \mathbf{F}_{\mathbf{contact}}(\mathbf{x}) \tag{16}$$

where $\ddot{\mathbf{x}}$, $\dot{\mathbf{x}}$ and $\mathbf{x}$ are the acceleration, velocity, and displacement response 15-dimensional vectors of the degrees-of-freedom, respectively. $\mathbf{F}_{\mathbf{pressure}}$ is the vector force due to net brake hydraulic pressure. $\mathbf{F}_{\mathbf{contact}}$ contains the linear and non-linear contact force terms at the stator and rotor interface and $\mathbf{F}_{\mathbf{couple}}$ defines the brake rod load. $\mathbf{M}$ is the structural mass matrix, $\mathbf{C}$ and $\mathbf{K}$ are the global damping and stiffness matrices of the system. They are given by

$$\mathbf{C} = \bar{\mathbf{C}} + \tilde{\mathbf{C}} \tag{17}$$

$$\mathbf{K} = \bar{\mathbf{K}} + \tilde{\mathbf{K}} \tag{18}$$

where $\bar{\mathbf{C}}$ and $\bar{\mathbf{K}}$ are the structural damping and stiffness matrices, and $\tilde{\mathbf{C}}$ and $\tilde{\mathbf{K}}$ define the damping and stiffness matrices due to the interconnections between each element.

The complete expression of the mass matrix $\mathbf{M}$, damping matrix $\mathbf{C}$ and stiffness matrix $\mathbf{K}$ are

$$\mathbf{M} = \begin{bmatrix} m_s & 0 & \cdots & \cdots & \cdots & \cdots & \cdots & \cdots & \cdots & \cdots & \cdots & \cdots & \cdots & \cdots & 0 \\ & I_{\theta s} & \ddots & & & & & & & & & & & & \vdots \\ & & I_{\psi s} & \ddots & & & & & & & & & & & \vdots \\ & & & I_{\varphi s} & \ddots & & & & & & & & & & \vdots \\ & & & & m_r & \ddots & & & & & & & & & \vdots \\ & & & & & I_{\theta r} & \ddots & & & & & & & & \vdots \\ & & & & & & I_{\psi r} & \ddots & & & & & & & \vdots \\ & & & & & & & m_b & \ddots & & & & & & \vdots \\ & & & & & & & & I_b & \ddots & & & & & \vdots \\ & & & & & & & & & m_b & \ddots & & & & \vdots \\ & & & & & & & & & & I_b & \ddots & & & \vdots \\ & & & & Sym. & & & & & & & m_a & \ddots & & \vdots \\ & & & & & & & & & & & & I_a & \ddots & \vdots \\ & & & & & & & & & & & & & m_a & 0 \\ & & & & & & & & & & & & & & I_a \end{bmatrix} \tag{19}$$

$$\mathbf{C} = \begin{bmatrix} C_{xs} & 0 & 0 & 0 & 0 & 0 & 0 & 0 & 0 & 0 & 0 & 0 & 0 & 0 & 0 \\ & C_{2,2} & 0 & 0 & 0 & 0 & 0 & 0 & 0 & 0 & 0 & 0 & -C_{as} & 0 & 0 \\ & & C_{3,3} & 0 & 0 & 0 & 0 & 0 & 0 & 0 & 0 & 0 & 0 & 0 & -C_{as} \\ & & & C_{\varphi s} & 0 & 0 & 0 & 0 & 0 & 0 & 0 & 0 & 0 & 0 & 0 \\ & & & & C_{xr} & 0 & 0 & 0 & 0 & 0 & 0 & 0 & 0 & 0 & 0 \\ & & & & & C_{6,6} & 0 & 0 & -C_{br} & 0 & 0 & 0 & 0 & 0 & 0 \\ & & & & & & C_{7,7} & 0 & 0 & 0 & -C_{br} & 0 & 0 & 0 & 0 \\ & & & & & & & C_{8,8} & C_{b12} & 0 & 0 & -C_{yab} & 0 & 0 & 0 \\ & & & & & & & & C_{9,9} & 0 & 0 & 0 & -C_{\theta ab} & 0 & 0 \\ & & & & & & & & & C_{10,10} & C_{b12} & 0 & 0 & -C_{zab} & 0 \\ & & & & & & & & & & C_{11,11} & 0 & 0 & 0 & -C_{\psi ab} \\ & & & Sym. & & & & & & & & C_{12,12} & C_{a12} & 0 & 0 \\ & & & & & & & & & & & & C_{13,13} & 0 & 0 \\ & & & & & & & & & & & & & C_{14,14} & C_{a12} \\ & & & & & & & & & & & & & & C_{15,15} \end{bmatrix} \tag{20}$$

with

$$
\begin{aligned}
C_{2,2} &= C_{as} + C_{\theta s} \\
C_{3,3} &= C_{as} + C_{\psi s} \\
C_{6,6} &= C_{br} + C_{\theta r} \\
C_{7,7} &= C_{br} + C_{\psi r} \\
C_{8,8} &= C_{b11} + C_{yab} \\
C_{9,9} &= C_{b22} + C_{br} + C_{\theta ab} \\
C_{10,10} &= C_{b11} + C_{zab} \\
C_{11,11} &= C_{b22} + C_{br} + C_{\psi ab} \\
C_{12,12} &= C_{a11} + C_{yab} \\
C_{13,13} &= C_{a22} + C_{as} + C_{\theta ab} \\
C_{14,14} &= C_{a11} + C_{zab} \\
C_{15,15} &= C_{a22} + C_{as} + C_{\psi ab}
\end{aligned}
\tag{21}
$$

$$
\mathbf{K} = \begin{bmatrix}
K_{hyd} & 0 & 0 & 0 & 0 & 0 & 0 & 0 & 0 & 0 & 0 & 0 & 0 & 0 & 0 \\
 & K_{2,2} & 0 & 0 & 0 & 0 & 0 & 0 & 0 & 0 & 0 & 0 & -K_{as} & 0 & 0 \\
 & & K_{3,3} & 0 & 0 & 0 & 0 & 0 & 0 & 0 & 0 & 0 & 0 & 0 & -K_{as} \\
 & & & 0 & 0 & 0 & 0 & 0 & 0 & 0 & 0 & 0 & 0 & 0 & 0 \\
 & & & & K_{rr} & 0 & 0 & 0 & 0 & 0 & 0 & 0 & 0 & 0 & 0 \\
 & & & & & K_{br} & 0 & 0 & -K_{br} & 0 & 0 & 0 & 0 & 0 & 0 \\
 & & & & & & K_{br} & 0 & 0 & 0 & -K_{br} & 0 & 0 & 0 & 0 \\
 & & & & & & & K_{8,8} & K_{b12} & 0 & 0 & -K_{yab} & 0 & 0 & 0 \\
 & & & & & & & & K_{9,9} & 0 & 0 & 0 & -K_{\theta ab} & 0 & 0 \\
 & & & & & & & & & K_{10,10} & K_{b12} & 0 & 0 & -K_{zab} & 0 \\
 & & & & & & & & & & K_{11,11} & 0 & 0 & 0 & -K_{\psi ab} \\
 & & & \textit{Sym.} & & & & & & & & K_{12,12} & K_{a12} & 0 & 0 \\
 & & & & & & & & & & & & K_{13,13} & 0 & 0 \\
 & & & & & & & & & & & & & K_{14,14} & K_{a12} \\
 & & & & & & & & & & & & & & K_{15,15}
\end{bmatrix}
\tag{22}
$$

with

$$
\begin{aligned}
K_{2,2} &= K_{as} + K_{\theta s} \\
K_{3,3} &= K_{as} + K_{\psi s} \\
K_{8,8} &= K_{b11} + K_{yab} \\
K_{9,9} &= K_{b22} + K_{br} + K_{\theta ab} \\
K_{10,10} &= K_{b11} + K_{zab} \\
K_{11,11} &= K_{b22} + K_{br} + K_{\psi ab} \\
K_{12,12} &= K_{a11} + K_{yab} \\
K_{13,13} &= K_{a22} + K_{as} + K_{\theta ab} \\
K_{14,14} &= K_{a11} + K_{zab} \\
K_{15,15} &= K_{a22} + K_{as} + K_{\psi ab}
\end{aligned}
\tag{23}
$$

K_{as} and C_{as} define the stiffness and the damping between the stator and the shaft of the stator, called torque tube, via notches on the inner perimeter of the disk. K_{br} and C_{br} define the stiffness and the damping between the rotor and the shaft of the rotor, via drive keys on the outside of the disk. $K_{\psi ab}$, $K_{\theta ab}$, K_{yab}, K_{zab} and $C_{\psi ab}$, $C_{\theta ab}$, C_{yab}, C_{zab} represent the contact stiffness and the contact damping between the rotor's and stator's shaft, respectively. K_{rr} represents the stiffness of the backplate of the brake. K_{aij} $(i, j = 1,2)$ and C_{aij} $(i, j = 1,2)$ are the axle bend stiffness and axle bend damping for the stator's shaft, respectively. K_{bij} $(i, j = 1,2)$ and C_{bij} $(i, j = 1,2)$ are the axle bend stiffness and axle bend damping for the rotor's shaft, respectively.

Finally, the general form of the equation of motion for the non-linear system can be expressed in the following way:

$$
\mathbf{M}\ddot{\mathbf{x}} + \mathbf{C}\dot{\mathbf{x}} + \left(\mathbf{K} - \hat{\mathbf{K}}\right)\mathbf{x} = \mathbf{F}_{\mathbf{pressure}} + \mathbf{F}_{\mathbf{contact}}\left(\mathbf{x}\right) \tag{24}
$$

with $\mathbf{F}_{\mathbf{couple}}\left(\mathbf{x}\right) = \hat{\mathbf{K}}\mathbf{x}$. Finally, a non-linear *15*-degree-of-freedom whirl system is defined (Sinou [6]). It has the form

$$
\mathbf{M}\ddot{\mathbf{x}} + \mathbf{C}\dot{\mathbf{x}} + \widehat{\mathbf{K}}\mathbf{x} = \mathbf{F}_{\mathbf{pressure}} + \mathbf{F}_{\mathbf{NL}}\left(\mathbf{x}\right) \tag{25}
$$

where $\ddot{\mathbf{x}}$, $\dot{\mathbf{x}}$ and $\mathbf{x}$ are the acceleration, velocity, and displacement response 15-dimensional vectors of the degrees-of-freedom, respectively. $\mathbf{M}$ is the mass matrix, $\mathbf{C}$ is the damping matrix and $\hat{\mathbf{K}}$ is the stiffness matrix. $\mathbf{F}_{\mathbf{pressure}}$ is the vector force due to brake command and $\mathbf{F}_{\mathbf{NL}}$ contains the quadratic and cubic non-linear terms.

Now we move on to the static problem and the stability analysis: the steady-state operating point for the full set of non-linear equations is obtained by solving them for the equilibrium point. Stability is investigated by determining the eigenvalues of the Jacobian matrix of the linearized system at the equilibrium point.

4 STABILITY ANALYSIS

The first step is the static problem: the steady state operating point for the full set of non-linear equations is obtained by their solution at the equilibrium point. Stability is investigated by calculating the Jacobian of the system at the equilibrium point [17-19]. This equilibrium point $\mathbf{x_0}$ is obtained by solving the non-linear static equations for a given net brake hydraulic pressure. This equilibrium point satisfies the following conditions:

$$
\widehat{\mathbf{K}}\mathbf{x_0} = \mathbf{F}_{\mathbf{pressure}} + \mathbf{F}_{\mathbf{NL}}\left(\mathbf{x_0}\right) \tag{26}
$$

The stability is investigated by calculating the Jacobian matrix $\mathbf{J}$ of the system at the equilibrium points; $\mathbf{J}$ is expressed by

$$\mathbf{J} = \begin{bmatrix} \mathbf{0} & \mathbf{I} \\ -\mathbf{M}^{-1}\left(\hat{\mathbf{K}} - \mathbf{K_L}\left(\mathbf{x_0}\right)\right) & -\mathbf{M}^{-1}\mathbf{C} \end{bmatrix} \tag{27}$$

where $\mathbf{K_L}\left(\mathbf{x_0}\right)$ defines the matrix of the linearized expressions of the non-linear terms contained by $\mathbf{F_{NL}}$ at the equilibrium point.

The eigenvalues of the constant matrix $\mathbf{J}$ provide information about the local stability of the equilibrium point $\mathbf{x_0}$. Considering λ the eigenvalues of the Jacobian matrix, it can be expressed as

$$\lambda = a + i.b \tag{28}$$

where a is the real part, and b is the imaginary part of the eigenvalue. If a is negative or zero, the system is stable and there is no vibration. If a is positive, we have an unstable root and whirl vibration. Therefore, b represents frequency of the unstable mode. The basic parameters chosen for the parametric studies are: $\mu/\mu_{max} = 0.33$; $P/P_{max} = 0.3$; $\alpha/\alpha_{max} 0.0875$; $\eta/\eta_{max} = 0.04$; $K_{rr}/K_{rr\,max} = 0.78$.

A representation of the evolution of frequencies and the evolution of the associated real part against the brake friction coefficient are given in Figures 16-17, and Figure 18, respectively. A representation of the evolution of the eigenvalues in the complex plane against the brake friction coefficient is given in Figure 16. As long as the real part of all the eigenvalues remains negative, the system is stable. When at least one of the eigenvalues has a positive real part, the dynamical system is unstable. This analysis indicates that system instability can occur with a constant friction coefficient. One observes that the system is generally stable at low values of the brake friction coefficient and unstable at high values. The frequency of instability is obtained near 250Hz, as shown in Figures 17 and 19. Moreover, it is possible to obtain the analytical mode shape associated to this instability for one period, as illustrated in Figure 20. Markers ① to ⑥ indicate the evolution of the mode shape. In this case, we observe a wobbling motion between the brake's rotating and stationary parts and this mode is defined as one wherein the cantilevered end of the torque plaque orbits about the axle. The shaded mark defines the static position of the aircraft brake system. As previously observed in the experimental results, an axial deflection of the axle tube and a complex rotating-bending motion of the rotor/stator stack is obtained (indicated by the whirling motion of the torque plate and the piston housing at the top and bottom of the aircraft brake system). So the analytical motion observed for instability near 250Hz is the same as the experimental deformation (observed in Figure 8) and defines the standard characteristics of whirl instability. Finally, it may be observed that there is a perfect correlation with experimental tests where the frequency of instability is between 240-280Hz.

In addition, an important point is determining the Hopf bifurcation point, defined as follows

$$\begin{aligned} &\mathrm{Re}\left(\lambda_{center}\left(\mu\right)\right)\Big|_{\mathbf{x}=\mathbf{x_0},\mu=\mu_0} = 0 \\ &\mathrm{Re}\left(\lambda_{non-center}\left(\mu\right)\right)\Big|_{\mathbf{x}=\mathbf{x_0},\mu=\mu_0} \neq 0 \\ &\frac{d}{d\mu}\left(\mathrm{Re}\left(\lambda\left(\mu\right)\right)\right)\Big|_{\mathbf{x}=\mathbf{x_0},\mu=\mu_0} \neq 0 \end{aligned} \tag{29}$$

The first condition implies that the system (25) has a pair of purely imaginary eigenvalues λ_{center} while all of its other eigenvalues $\lambda_{non-center}$ have nonzero real parts at $\left(\mathbf{x} = \mathbf{x_0}, \mu = \mu_0\right)$. The last condition of equation (29), called a transversal condition, implies a transversal or nonzero speed crossing of the imaginary axis, as shown in Figure 18.

In order to avoid whirl instability and to understand the influence of various parameters, parametric studies may be investigated. In the following study, two parameters will be developed.

First, Figures 21-26 illustrate the evolution of the static position for various parametric studies. It may be observed that for each parameter a correct determination of the equilibrium point is essential to estimate the stability of the system obtained by determining the eigenvalues of the matrix (27). Moreover, these results indicate that the non-linear compression behavior of the rotor/stator stack is important in order to avoid incorrect diagnostic for stability analysis.

Then, Figures 21 and 22 indicate that the normal static position of the stator x_S is only dependent on the normal brake pressure and that the piston torsional rotation φ_S is dependant both on the friction coefficient and the

brake pressure. Figures 23 and 24 illustrate that the normal static position x_S and the piston torsional rotation φ_S are more dependant for the brake pressure than for the offset angle. Then, Figures 25 and 26 illustrate the evolution of the static positions x_S and φ_S by considering variations of the offset angle and friction coefficient. The contribution and influence of these last two parameters appears to be of the same order. However, the global variation of the normal static position of the stator x_S is less important than in the two previous cases where the brake pressure was considered. So it may be concluded that the static equilibrium point is greatly and firstly affected by the brake pressure but that all parameters affect the static position that need to be precisely determined in order to undertake a correct stability analysis

Figure 27 shows whirl stability analysis versus the brake friction coefficient and the brake pressure. As indicated in Figure 28, whirl instability is in the range 235-255Hz. It may be observed that increasing the brake pressure ($P/P_{max} > 0.2$) increases the value of the Hopf bifurcation point (versus the brake friction parameter). However, the whirl instability may not be eliminated if the brake friction coefficient is greater than $\mu/\mu_{max} > 0.42$. Then, decreasing the brake pressure ($P/P_{max} < 0.2$) decreases the unstable zone associated with the whirl instability. It may be observed that, for a given brake pressure and by increasing the friction coefficient, the system is first stable, then becomes unstable, and finally is stable again. So the whirl instability may be avoided if the friction coefficient is high with a low brake pressure(for example $\mu/\mu_{max} > 0.9$ and $P/P_{max} < 0.2$).

However, in this case, another instability appears, as indicated in Figures 29-30. This instability appears only for low pressure (less than the basic brake pressure, $P/P_{max} < 0.2$) and is in the range 450-800Hz. So decreasing the nominal brake pressure may not be applied in order to avoid whirl instability due to the fact that the whirl instability may be eliminated but another instability may appear.

Figures 31 and 32 illustrate whirl stability analysis versus the brake friction coefficient and the offset angle (and by keeping the nominal brake pressure $P/P_{max} = 0.2$). Figures 33 and 34 indicate the whirl stability analysis versus the brake pressure and the offset angle (and by keeping the brake friction coefficient pressure $\mu/\mu_{max} = 0.33$). In both cases, the system is stable only if the brake friction coefficient and the offset angle, and the brake pressure and the offset angle are very small. So it will be very difficult to obtain these conditions for physical cases. In these cases, the whirl instability is around 250-260Hz and 220-260 Hz for the first and second parametric studies, as illustrated in Figures 32 and 34, respectively.

In a broad variety of engineering systems, incorporating additional damping into one part of the brake system is undertaken in order to significantly reduce or eliminate friction-induced vibrations. We now proceed with two parametric studies in order to evaluate this design solution. First, Figure 35 and 36 illustrate whirl stability analysis versus the brake friction coefficient and the damping coefficient of the torque plate. Second, Figure 37 and 38 illustrate whirl stability analysis versus the brake pressure and the damping coefficient of the torque plate. At low damping ($\eta/\eta_{\max} < 0.2$), the whirl instability is detected around 230-260Hz. But, the whirl instability disappears by adding damping on the torque plate ($\eta/\eta_{\max} > 0.2$), as illustrated in Figures 35 and 37. However, in these cases, the aircraft brake system may have another instability if damping is added on the torque plate, as illustrated in Figures 39-42. These instabilities occur near 750-780Hz and 450-700Hz.. So it may be concluded that increasing damping may destabilize friction-induced vibrations and that the role of structural damping is not a secondary effect that can be ignored. In these last two parametric studies it has been illustrated that adding damping into one part of the mechanical systems may have a worse effect [20-22] and cannot be considered as a solution to avoid instability for the aircraft brake system.

Finally, two parametric studies consider the influence of the brake friction coefficient and the torque plate stiffness and the brake pressure and torque plate stiffness, respectively. Figures 43 and 44 show the associated stable and unstable zones. As indicated in Figures 45 and 46, the whirl instability is around 240-255Hz for the two parametric studies. Figures 43 and 44 clearly indicate that the stiffness of the torque plate plays an important role in the stability analysis of the aircraft brake system. If this stiffness is more flexible ($K_{rr}/K_{rr\ \max} < 0.68$) or stiffer ($K_{rr}/K_{rr\ \max} > 0.79$) than the nominal stiffness value of the torque plate, the whirl instability is eliminated and the aircraft brake system is stable (there is no other instability). So varying the stiffness value for

the torque plate may be considered as a design solution in order to avoid instabilities for the aircraft brake system.

5 SUMMARY AND CONCLUSION

A nonlinear model for the analysis of mode aircraft brake whirl has been developed by using experimental observations. Results from stability analysis are investigated by determining the Jacobian matrix of the non-linear system for each steady-state operating point. This stability analysis indicates that system instability can occur with a constant friction coefficient. A perfect correlation between the numerical model and the experimental tests is obtained for the frequency of instability and the deformation shape of the unstable mode.
Generally speaking, we observe that the aircraft brake system is stable at low values of brake friction coefficient and unstable at high values. Finally, parametric studies with linear stability theory are conducted in order to determine the effect of system parameters on stability. We see that the determination of the equilibrium point is essential in order to conduct a correct stability analysis. Moreover, it was demonstrated that eliminating instabilities for a mechanical system may be very difficult. More particularly, incorporating additional damping into one part of the aircraft brake system may have worse effects on the stability of the system.

ACKNOWLEDGMENTS

The authors would like to thank Messier-Bugatti for permission to publish this work.

REFERENCES

[1] S. Y Liu, M.A. Ozbek and J.T. Gordon. A Nonlinear Model for Aircraft Brake Squeal Analysis. Part i : Model Description and Solution Methodology. *In ASME Design Engineering Technical Conferences*, **3**, 1996, 406-416.

[2] S. Y Liu, M.A. Ozbek and J.T. Gordon. A Nonlinear Model for Aircraft Brake Squeal Analysis. Part ii : Stability Analysis and Parametric Studies. *In ASME Design Engineering Technical Conferences*, **3**, 1996, 417-425.

[3] J.T. Gordon. A Perturbation Analysis of Nonlinear Squeal Vibrations in Aircraft Braking Systems. *In ASME Design Engineering Technical Conferences*, **3**, 1996, 417-425.

[4] D.J. Feld, and D.J. Fehr. Complex Eigenvalue Analysis Applied to an Aircraft Brake Vibration Problem. *In ASME Design Engineering Technical Conferences*, 1997, 1-17.

[5] M.H. Travis. Nonlinear Transient Analysis of Aircraft Landing Gear Brake Whirl and Squeal. *In ASME Design Engineering Technical Conferences*, **3**, 1995, 1209-1216.

[6] R.A. Ibrahim 1994 *ASME Applied Mechanics Review*, 47, n°7, 209-226. Friction-Induced Vibration, Chatter, Squeal and Chaos : Part I - Mechanics of Contact and Friction.

[7] R.A. Ibrahim 1994 *ASME Applied Mechanics Review*, 47, n°7, 227-253. Friction-Induced Vibration, Chatter, Squeal and Chaos : Part II – Dynamics and Modeling.

[8] D.A. Crolla and A.M. Lang 1991 *Tribologie,* 18, Vehicle Tribology, 165-174.Brake Noise and Vibration – State of Art.

[9] N.M. Kinkaid, O.M. O'Reilly, P. Papadopoulos 2003 *Journal of Sound and Vibration*, 267, 105-166. Automobive disc brake squeal.

[10] J.T. Oden and J.A.C Martins 1985 *Computer Methods in Apllied Mechanics and Engineering*, 52, 527-634. Models and Computational Methods for Dynamic friction Phenomena.

[11] R.T. Spurr 1961 *Proc. Auto. Div. Instn. Mech. Engrs*, 33-40. A theory of brake squeal, 1961.

[12] R.P. Jarvis and B.Mills 1963/1964 *Proc. Instn. Mech. Engrs*, 178, n°32, 847-866. Vibrations induced by dry friction.

[13] S.W.E Earles and G.B. Soar 1971 *Proc.I.Mech.E.Conf. on "Vibration and Noise in Motor Vehicles"*, Paper C100/71. Squeal noise in disc brakes.

[14] Millner, 1978 *Society Automotive Engineer* Paper 780332. An Analysis of Disc Brake Squeal.

[15] M.R. North 1972 *14th FISITA congress*, Paper 1/9. A Mechanism of disc brake squeal.

[16] A.F. D'Souza and A.H. Dweib 1990 *Journal of Sound and Vibration*, 137(2), 177-190. Self-excited Vibrations induced by Dry Friction. Part 2: Stability and Limit-cycle Analysis.

[17] J-J. Sinou, Synthèse Non-Linéaire des Systèmes Vibrants – Application aux systèmes de freinage, Thèse de doctorat, Ecole Centrale de Lyon, 2002.
[18] J-J. Sinou, F. Thouverez, O. Dereure, and G-B. Mazet, Non-linear Dynamics of a Complex Aircraft Brake System – Experimental and Theorical Approaches..*In ASME Design Engineering Technical Conferences*, DETC2003/VIB-48579, *Chicago, Illinois*, 2003.
[19] J-J. Sinou, F. Thouverez, L. Jézéquel and G-B. Mazet, Friction, Instability and Parametric Studies of a Nonlinear Model for an Aircraft Brake Whirl Analysis, *In ASME Design Engineering Technical Conferences*, DETC2001/VIB-21726, *Pittsburgh, Pennsylvania*, 2001.
[20] S.W.E Earles and P.W. Chambers 1987 *Int. J. of vehicle Design*, 8, nos 4/5/6, 538-552.Disc Brake Squeal Noise generation : Predicting its Dependency on System parameters Including Damping.
[21] K. Shin, J-E. Oh, M.J. Brennan 2002 *JSME International Journal*, 45, 426-432. Nonlinear analysis of friction induced vibrations of a two degree of freedom model for disc brake squeal noise.
[22] K. Shin, M.J. Brennan J-E. Oh, C.J. Harris 2002 *Journal of Sound and Vibration*, 254, 837-848. Analysis of disc brake noise using a two-degree-of-freedom model.

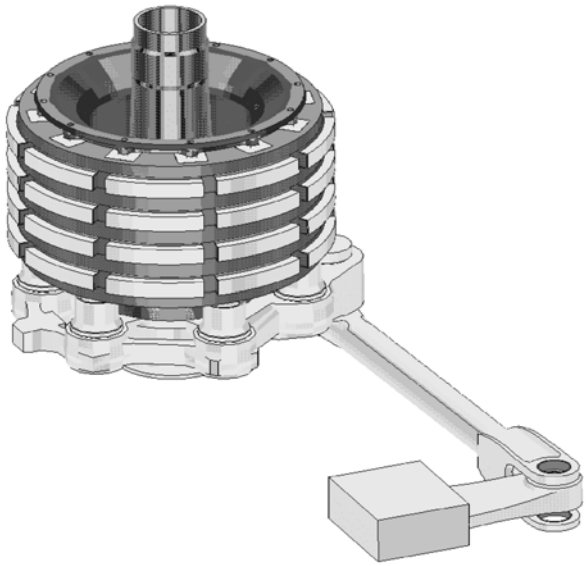

Figure 1 : Aircraft brake system

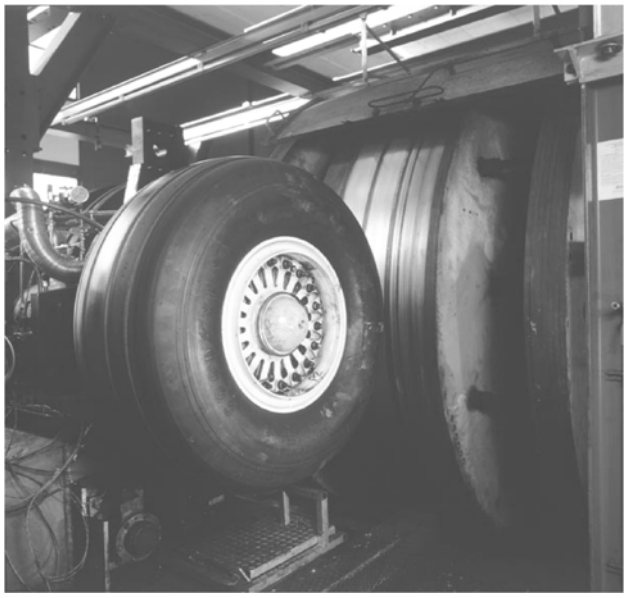

Figure 2 : Dynamic tests

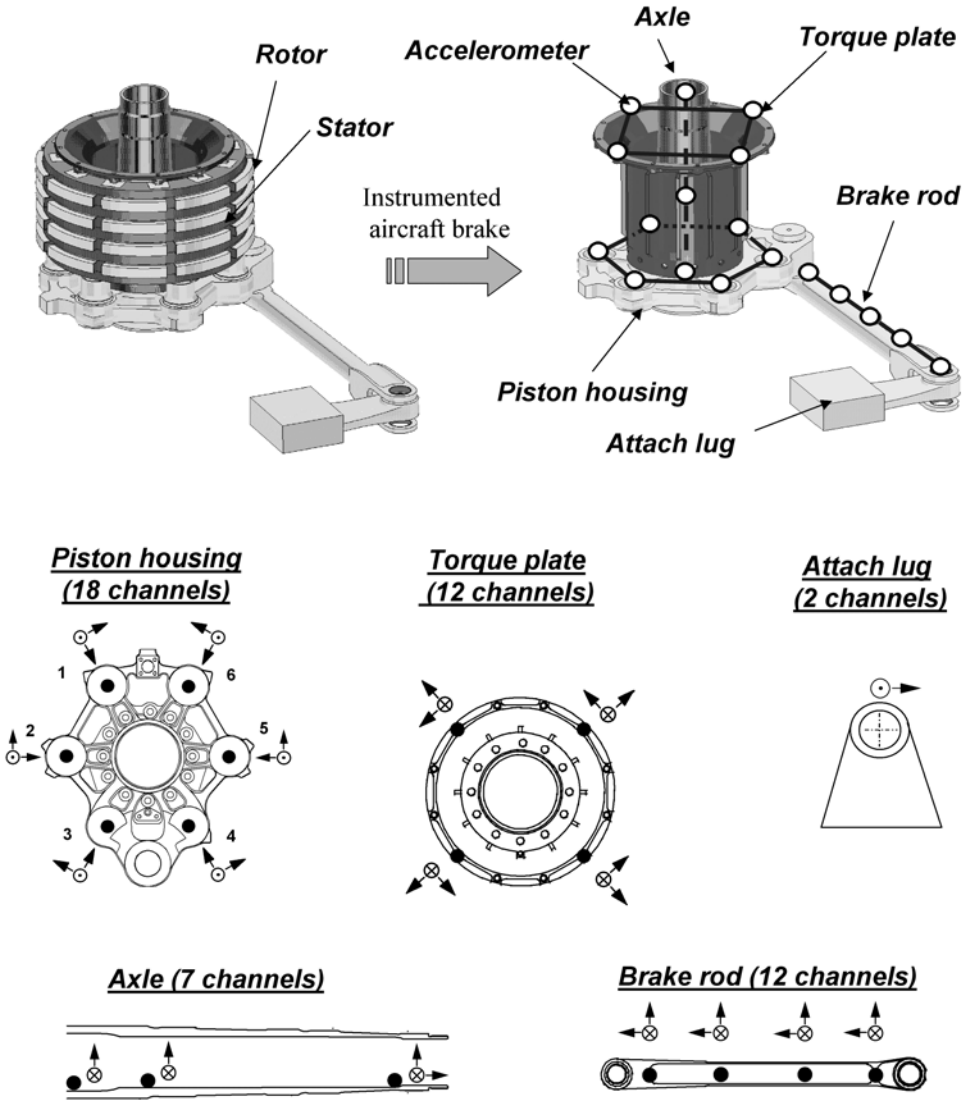

Figure 3: Instrumented aircraft brake

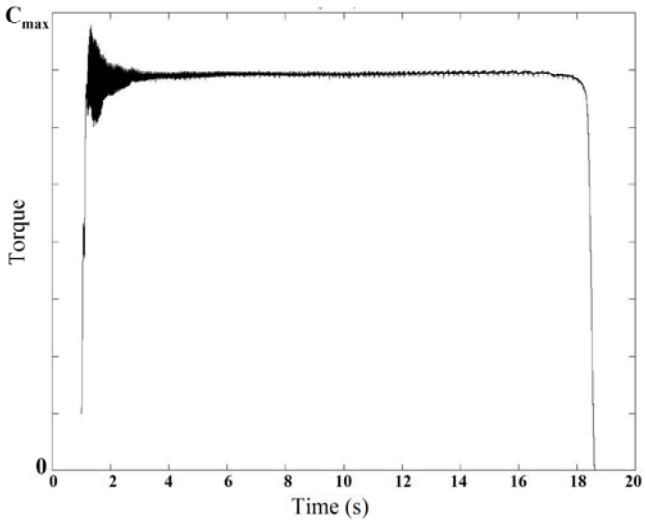

Figure 4 : Torques's time plot due to whirl vibration

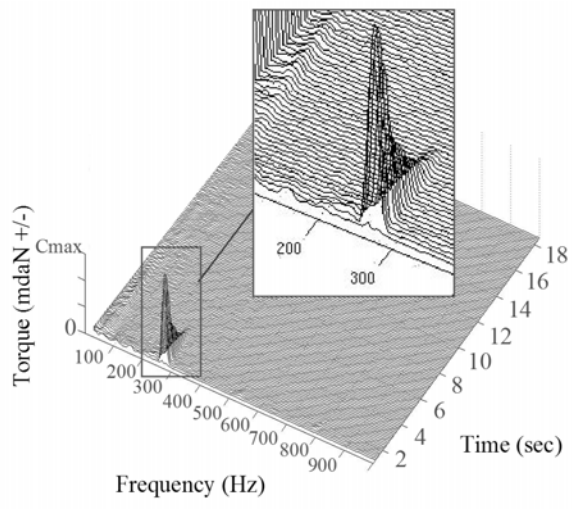

Figure 5: Torque's waterfall

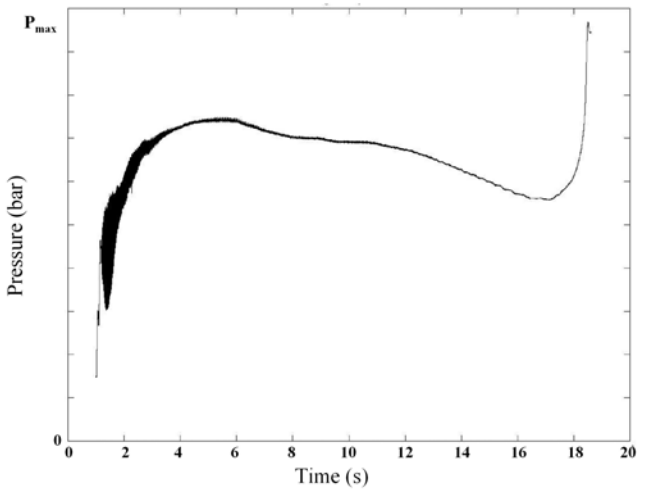

Figure 6 : Pressure's time plot due to whirl vibration

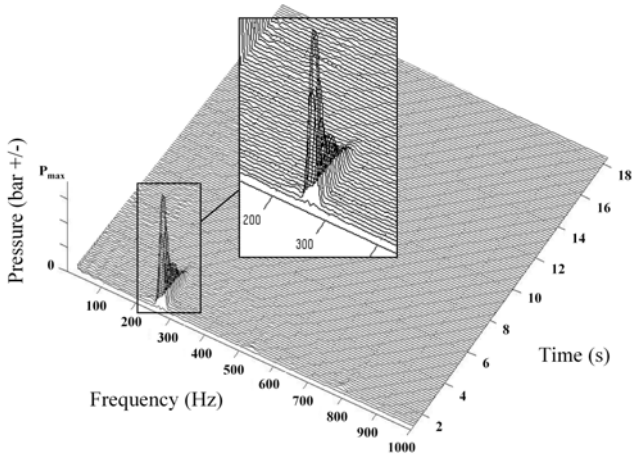

Figure 7: Pressure's waterfall

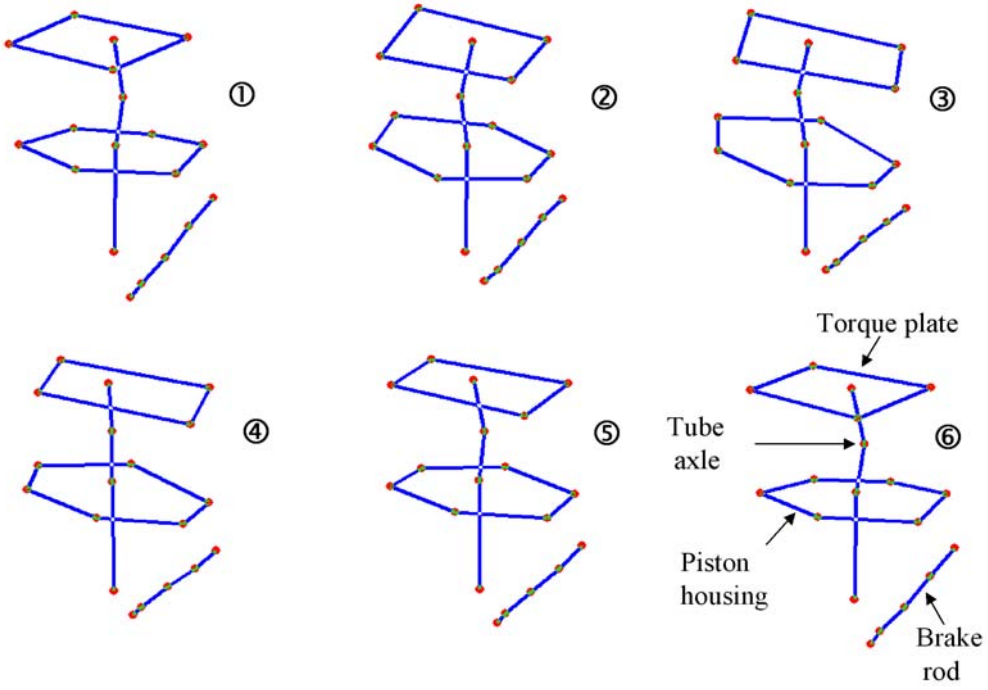

Figure 8 : Experimental deformation for the whirl

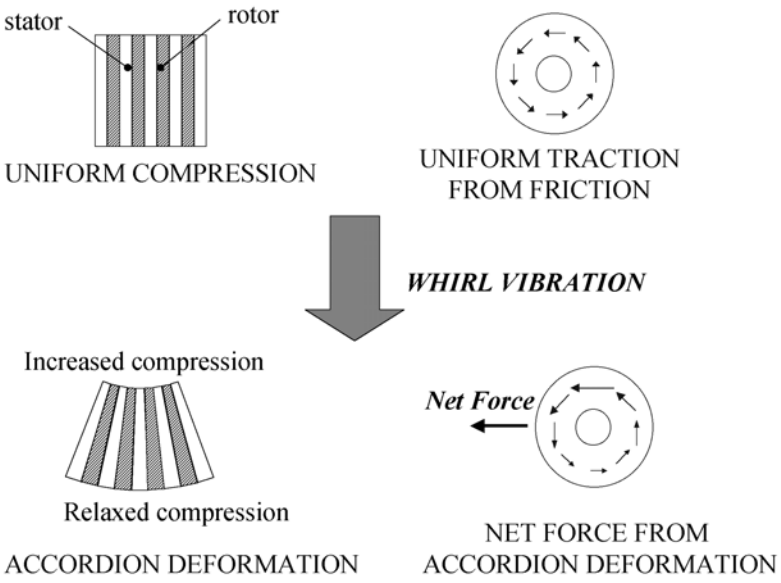

Figure 9 : Friction force variation on rubbed surface

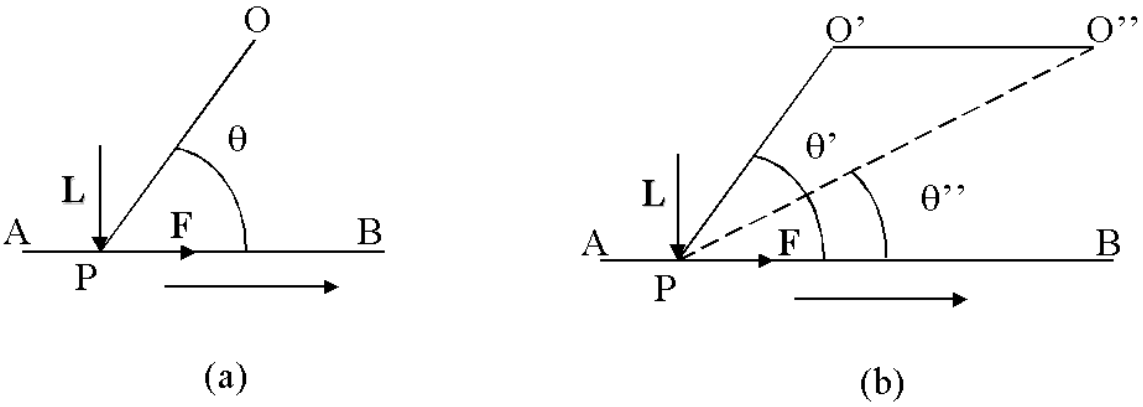

Figure 10: Sprag-slip model

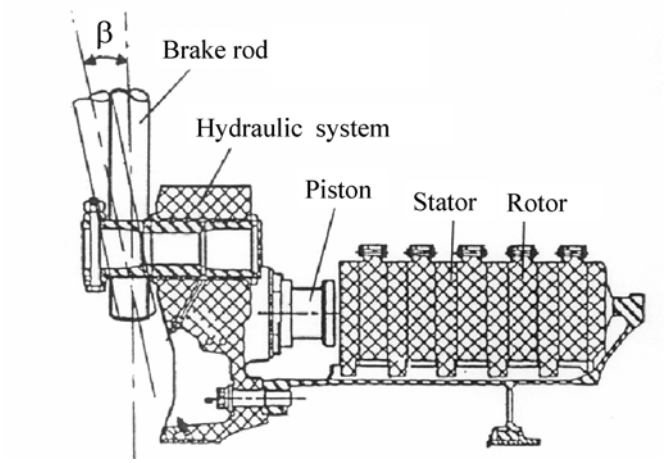

Figure 11: Offset angle β between the rod and the housing

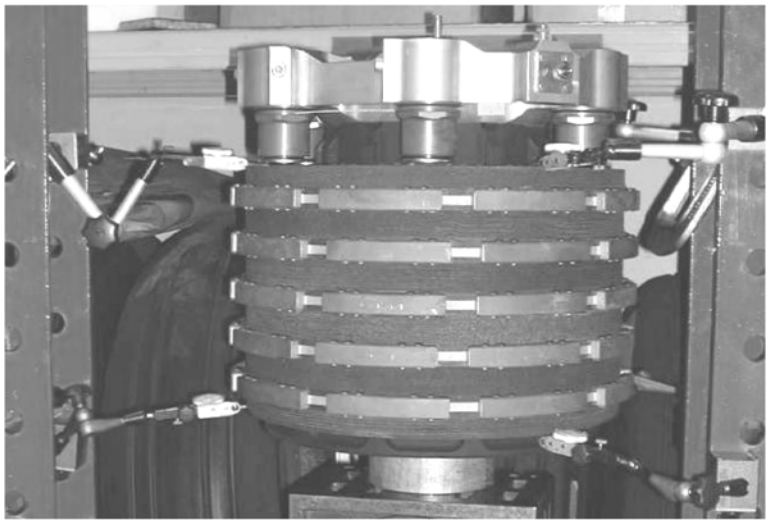

Figure 12: Static test

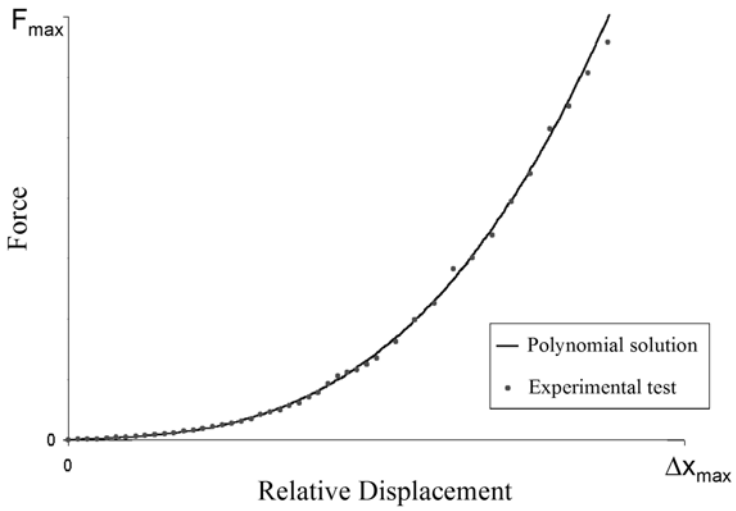

Figure 13 : Non-linear relationship between load and deflection experimental and theorical approaches

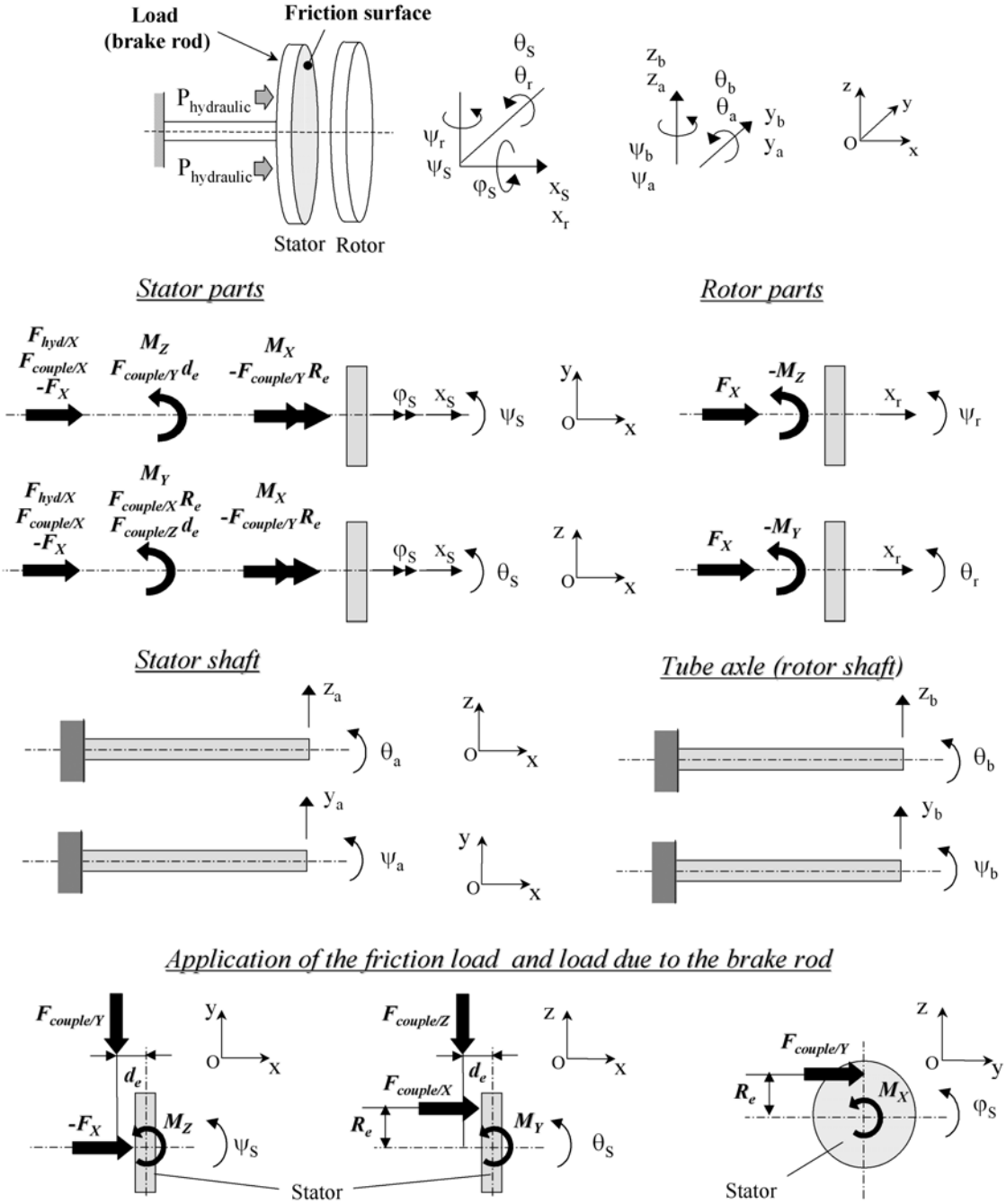

Figure 14 : Model of whirl vibration

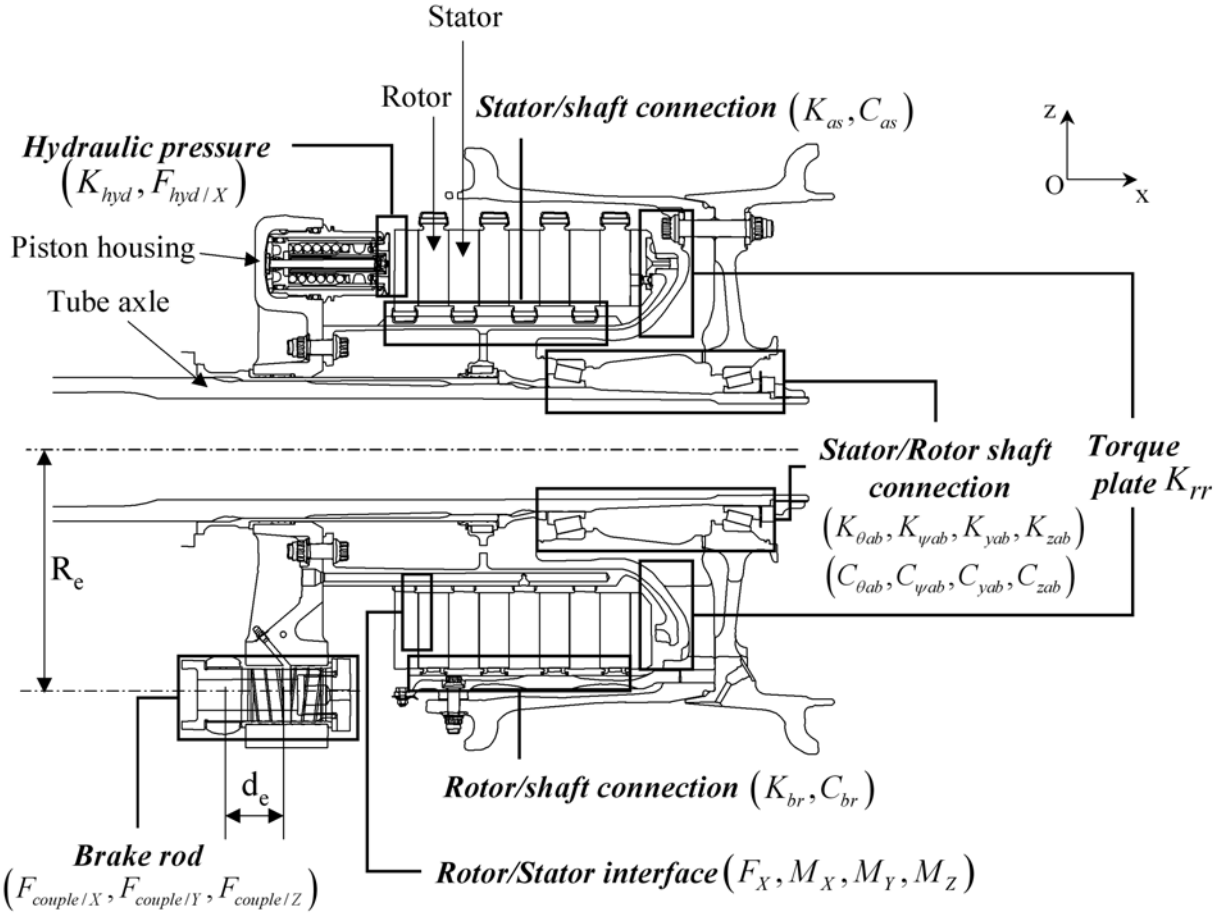

Figure 15 : Model of whirl vibration

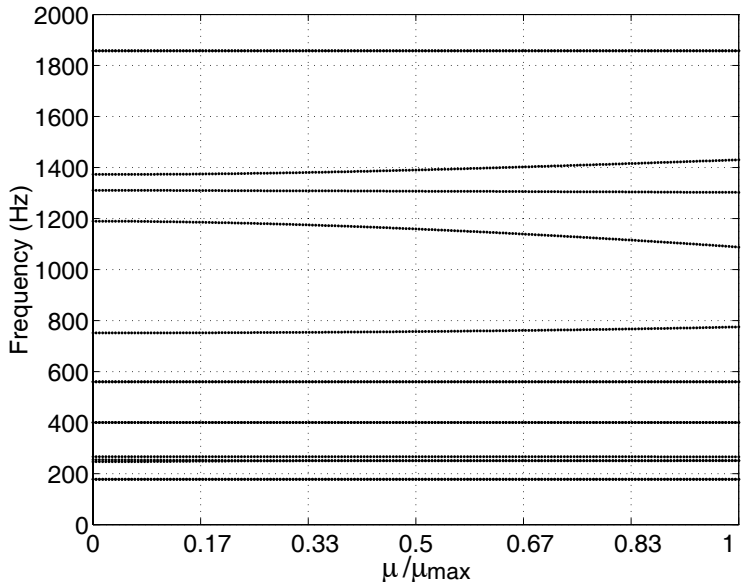

Figure 16: Evolution of the frequencies

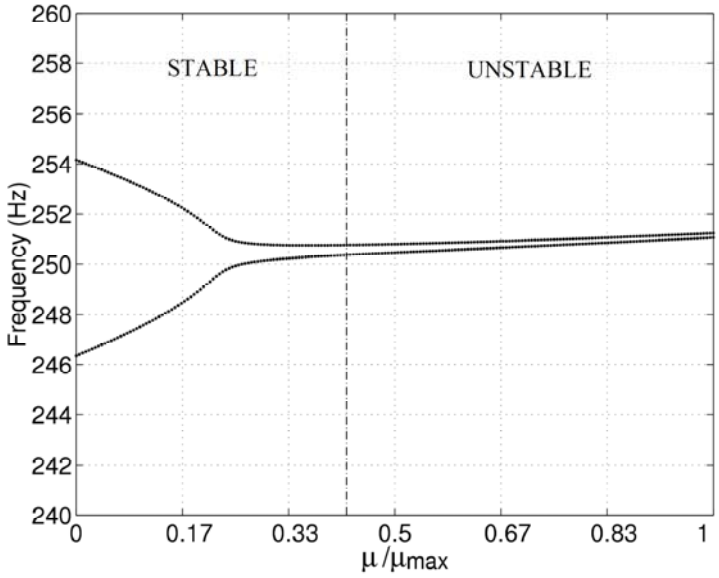

Figure 17: Coupling of two eigenvalues

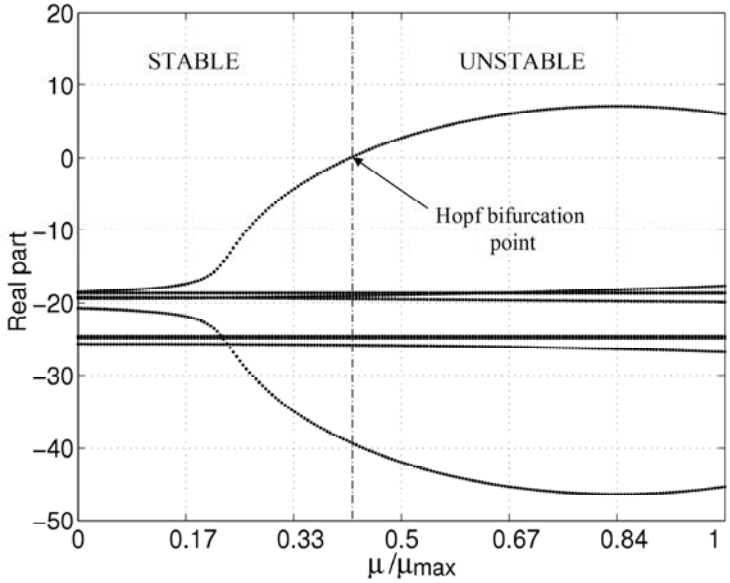

Figure 18: Evolution of the real part of two coupling modes

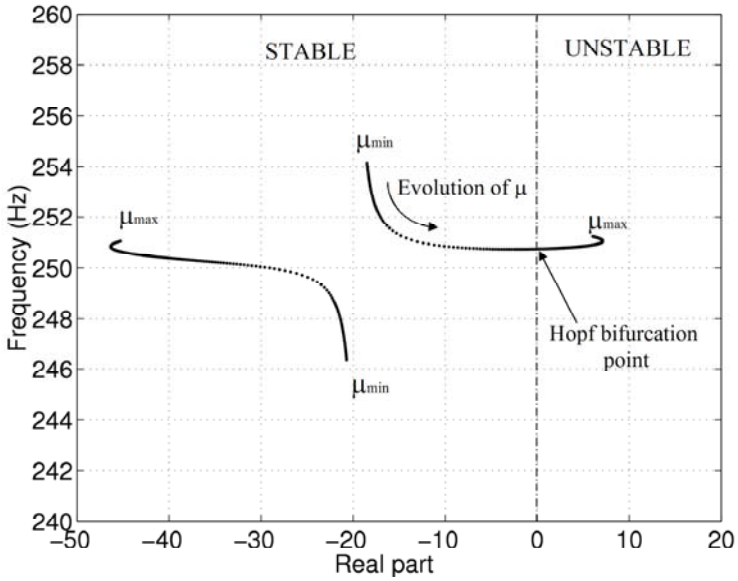

Figure 19: Evolution of the eigenvalues in the complex plane

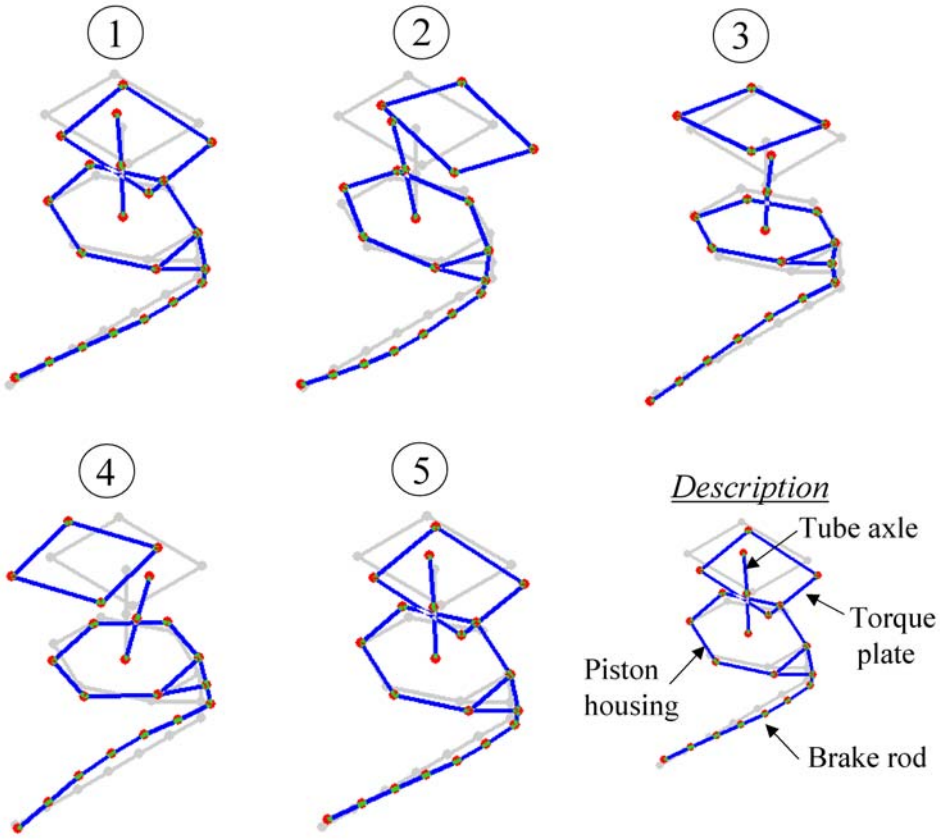

Figure 20: Analytical deformation of the whirl

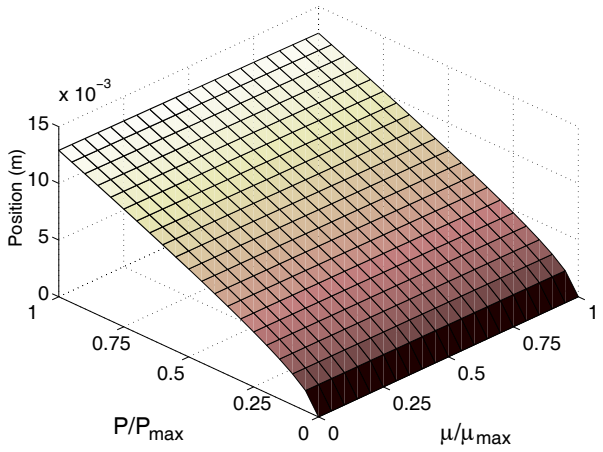

Figure 21: Evolution of the static equilibrium point x_s versus the brake friction coefficient and hydraulic pressure

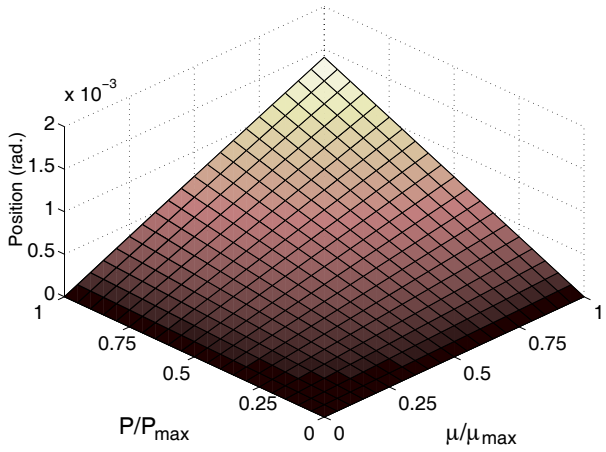

Figrue 22: Evolution of the static equilibrium point φ_s versus the brake friction coefficient and hydraulic pressure

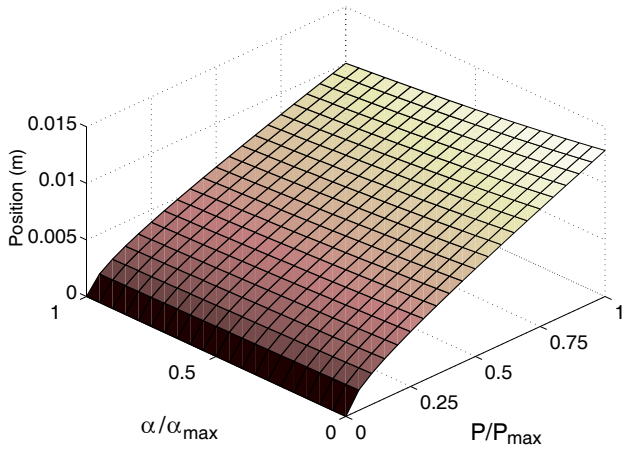

Figure 23: Evolution of the static equilibrium point x_s versus sprag-slip angle and the hydraulic pressure

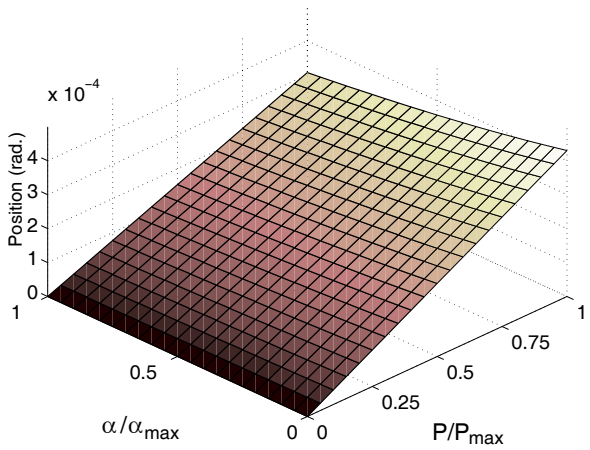

Figrue 24: Evolution of the static equilibrium point φ_s versus sprag-slip angle and the hydraulic pressure

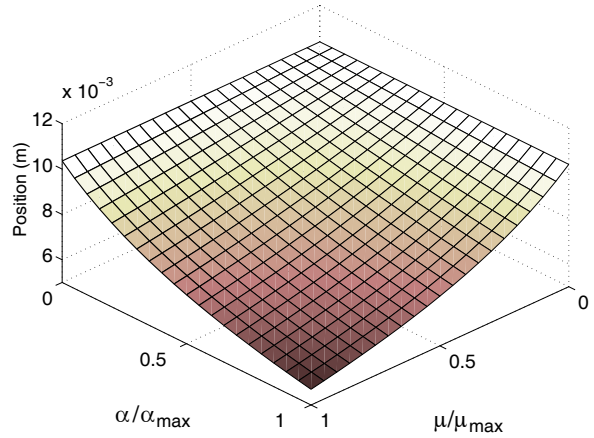

Figure 25: Evolution of the static equilibrium point x_s versus the brake friction coefficient and sprag-slip angle

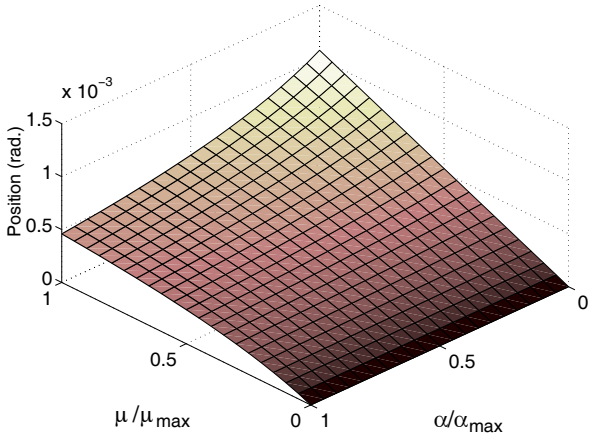

Figrue 26: Evolution of the static equilibrium point φ_s versus the brake friction coefficient and sprag-slip angle

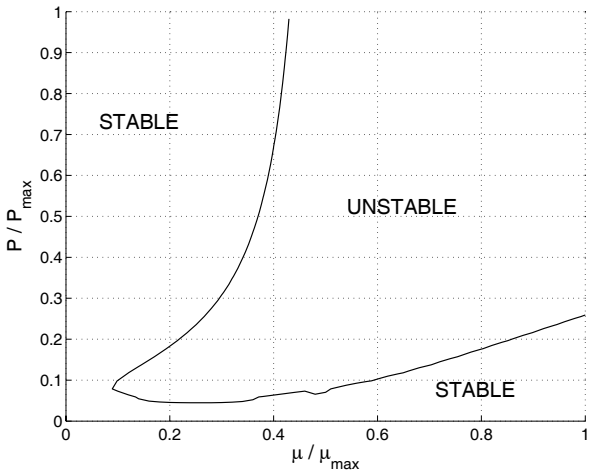

Figure 27: stability analysis versus the friction and the pressure for the whirl vibration

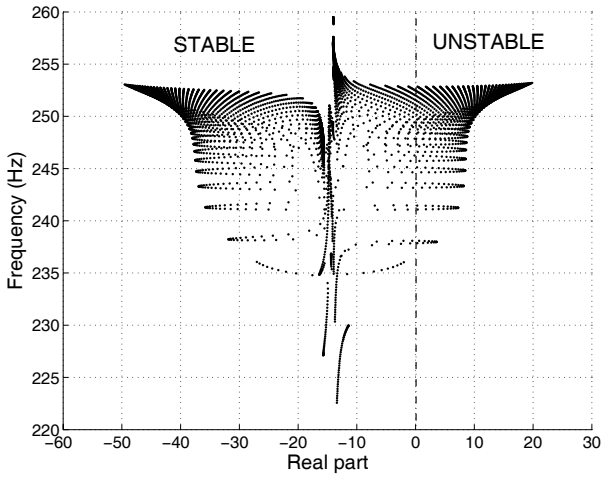

Figure 28: Evolution of the frequencies in the complex plane versus the friction and the pressure for the whirl vibration

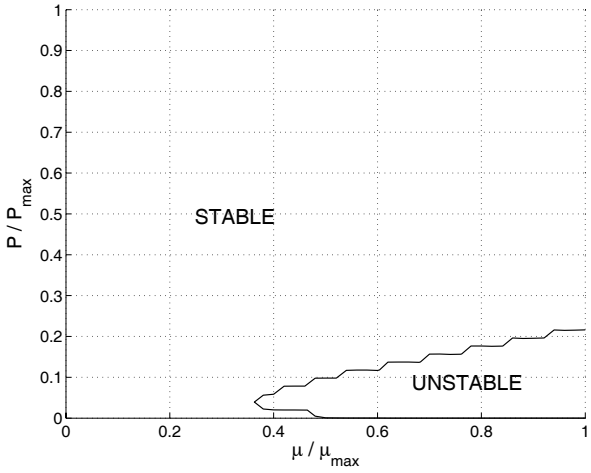

Figure 29: stability analysis versus the friction and the pressure around 400-900Hz

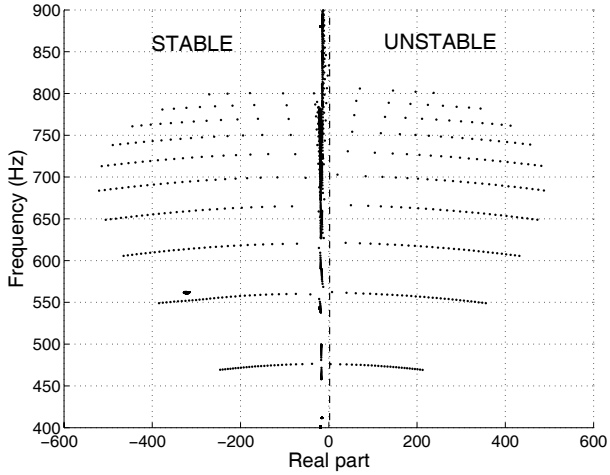

Figure 30: Evolution of the frequencies in the complex plane versus the friction and the pressure around 400-900Hz

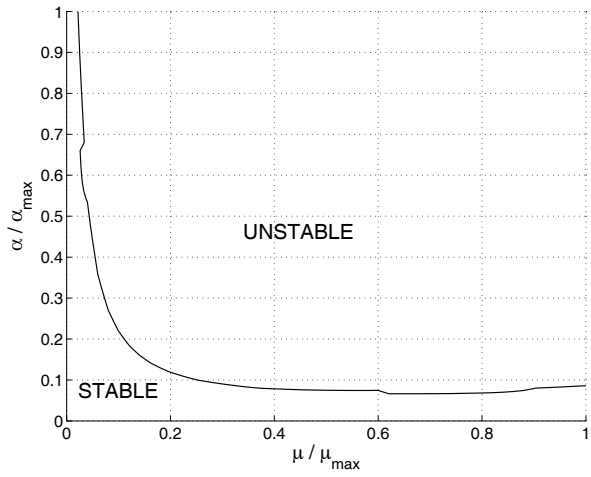

Figure 31: Stability analysis versus the friction and the angle

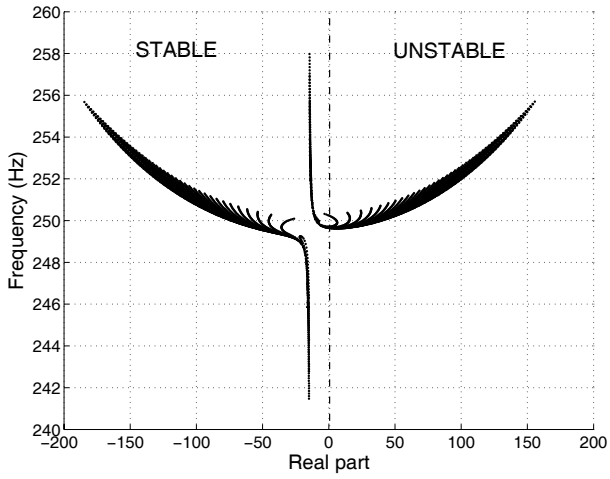

Figure 32: Evolution of the frequencies in the complex plane versus the friction and the angle

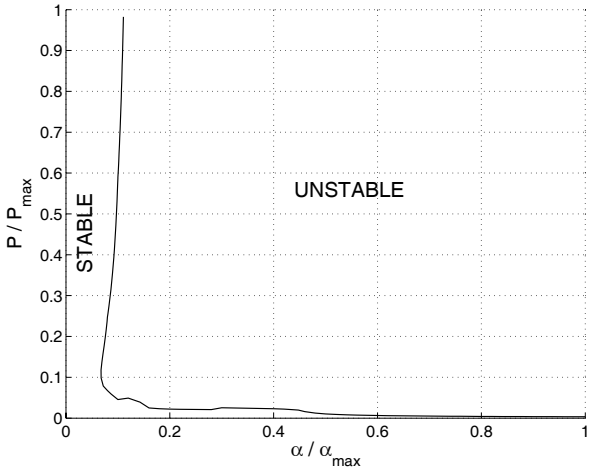

Figure 33: Stability analysis versus the pressure and the angle

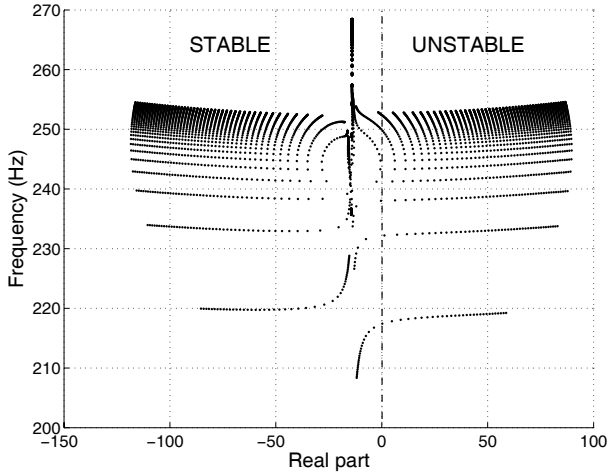

Figure 34: Evolution of the frequencies in the complex plane versus the pressure and the angle

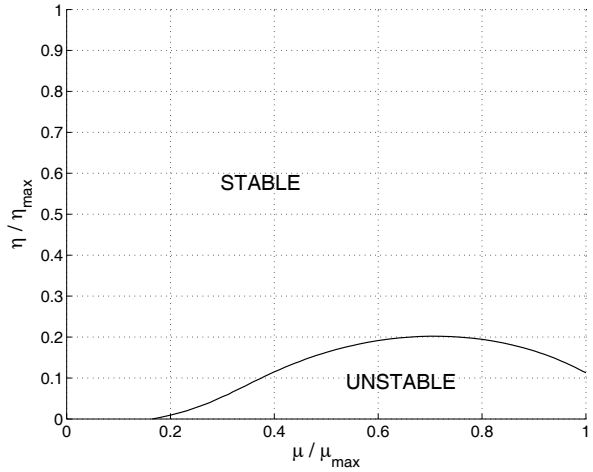

Figure 35: Stability analysis versus the friction and the damping for the whirl instability

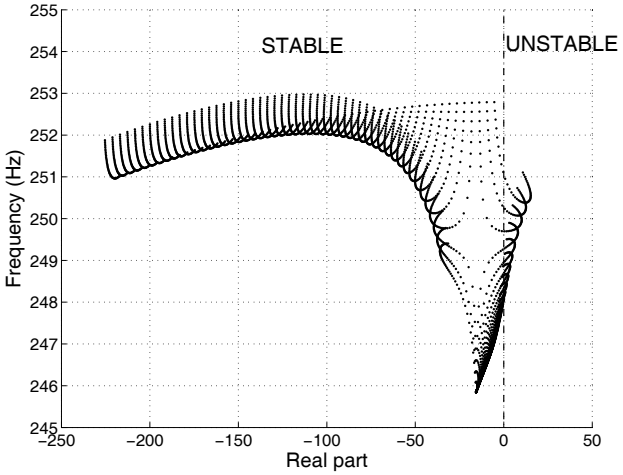

Figure 36: Evolution of the frequencies in the complex plane versus the friction and the damping for the whirl instability

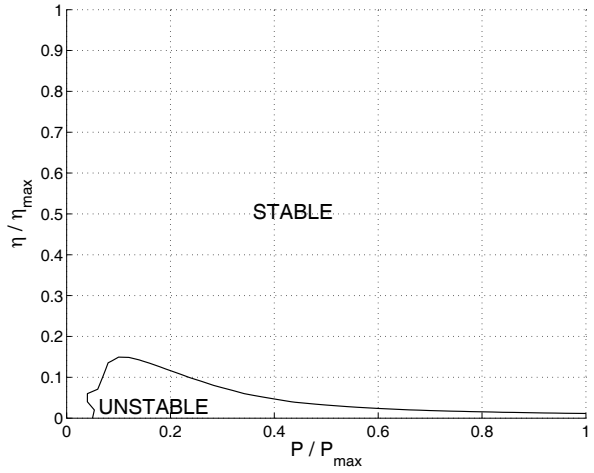

Figure 37: Stability analysis versus the pressure and the damping for the whirl instability

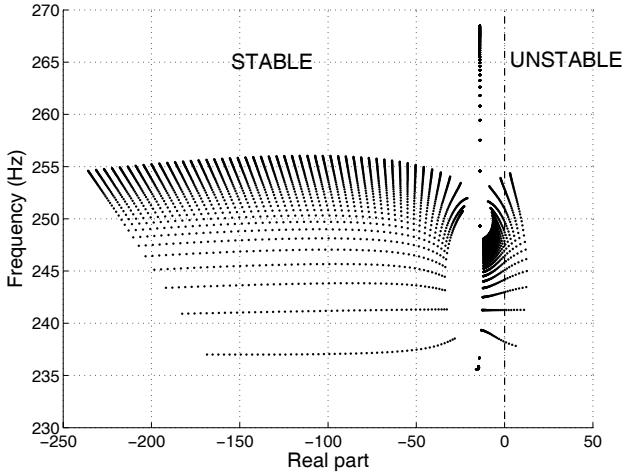

Figure 38: Evolution of the frequencies in the complex plane versus the pressure and the damping for the whirl instability

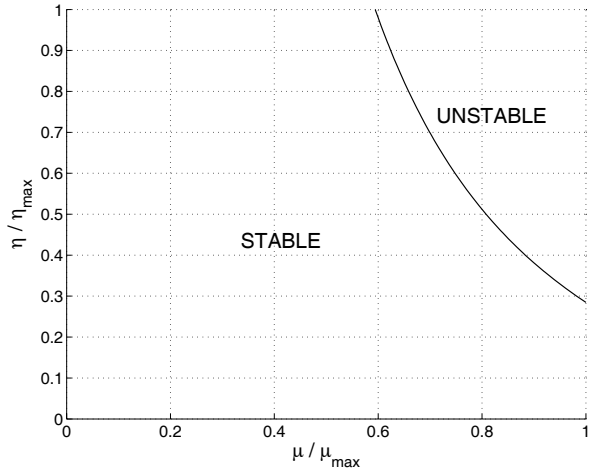

Figure 39: Stability analysis versus the friction and the damping around 700-800 Hz

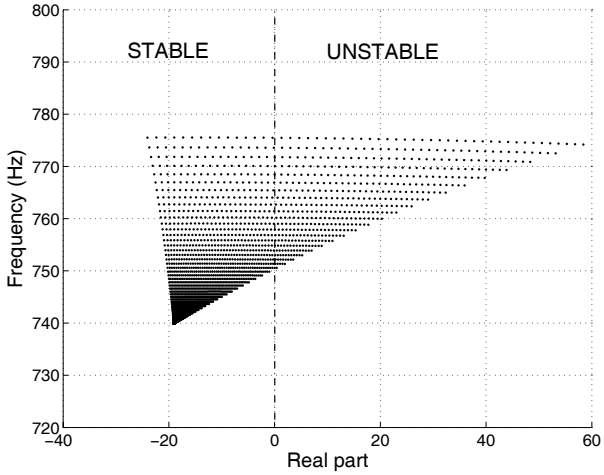

Figure 40: Evolution of the frequencies in the complex plane versus the friction and the damping around 700-800 Hz

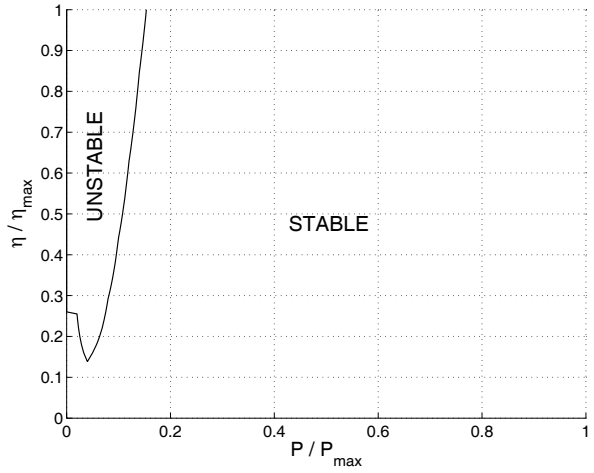

Figure 41: Stability analysis versus the pressure and the damping around 400-800 Hz

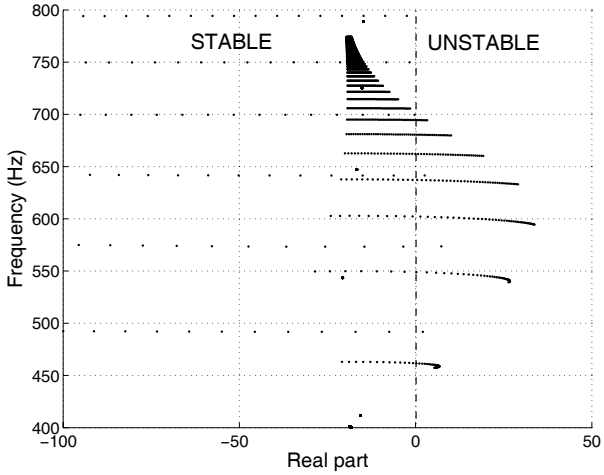

Figure 42: Evolution of the frequencies in the complex plane versus the pressure and the damping around 400-800 Hz

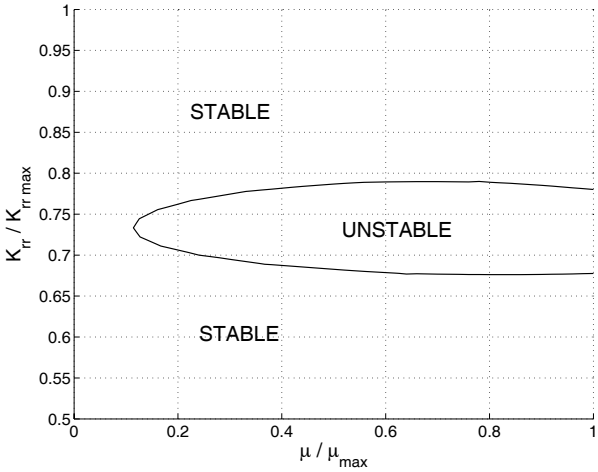

Figure 43: Stability analysis versus the friction and the stiffness of the backplate

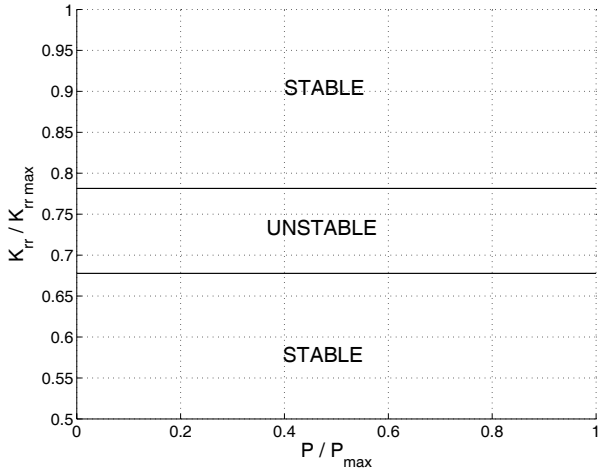

Figure 44: Stability analysis versus the pressure and the stiffness of the backplate

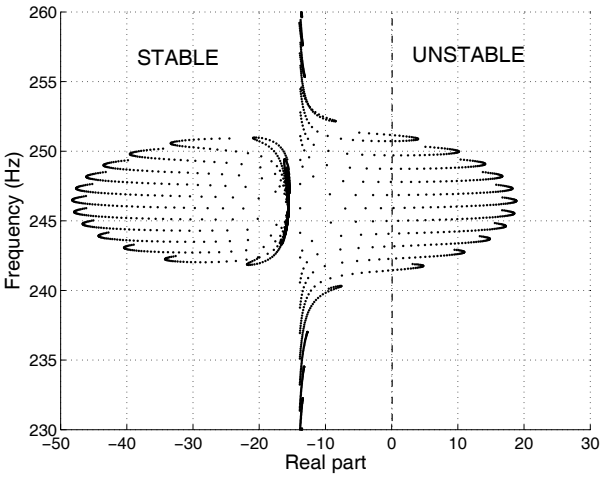

Figure 45: Evolution of the frequencies in the complex plane versus the friction and the stiffness of the backplate

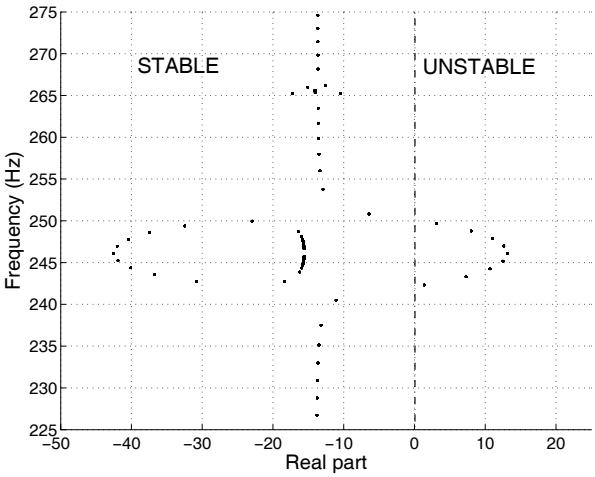

Figure 46: Evolution of the frequencies in the complex plane versus the pressure and the stiffness of the backplate